Supporting information

Tuning the stacking behaviour of a 2D covalent organic framework through non-covalent interactions

F. Haase, K. Gottschling, L. Stegbauer, L. S. Germann, R. Gutzler, V. Duppel, V. S. Vyas, K. Kern, R. E. Dinnebier, B. V. Lotsch

Methods:

Synthesis

*T*ris(4-formylphenyl)*t*riazine (TT-CHO) and *t*ris(4-aminophenyl)*t*riazine (TT-NH2) were synthesized according to literature procedures.[1] *T*ris(4-aminophenyl)*b*enzene (TB-NH2) was obtained from TCI Chemicals.

*T*riazine-*t*riazine-triphenyl-*i*mine (TTI-COF):[1] TT-CHO (0.0635 mmol, 25.0 mg), TT-NH2 (0.0635 mmol, 22.5 mg), mesitylene (2.5 ml), 1,4-dioxane (2.5 ml), aqueous acetic acid (0.794 mmol, 6M, 0.132 ml) were added successively to a Biotage© precision glass vial, sealed and heated under autogenous pressure at 120°C for 72 h. After the reaction was allowed to cool down, the reaction mixture was filtered and washed thoroughly with ethanol, water, tetrahydrofuran and chloroform and then dried in high dynamic vacuum overnight.

*T*riazine *b*enzene triphenyl *i*mine (TBI-COF): TB-NH2 (0.032 mmol, 12.1 mg), TT-CHO (0.032 mmol, 12.6 mg), mesitylene (0.5 ml), 1,4-dioxane (0.5 ml), aqueous acetic acid (6M, 0.5 ml) were added successively to a Biotage© precision glass vial, sealed and heated under autogenous pressure at 155°C for 45 min. Afterwards the reaction vial was placed in a muffle furnace and heated at 120°C for 72 h. After the reaction was allowed to cool down, the reaction mixture was filtered and washed thoroughly with dimethylformamide, tetrahydrofuran and dichloromethane and then dried in a desiccator.

Model construction

Models of the structures were produced in Materials Studio v6.0.0 Copyright © 2011 Accelrys Software using of the Forcite Geometry optimizations with universal force fields with Ewald electrostatic and van der Waals summations methods.

SEM

SEM SE (secondary electron) detector images were obtained on either a Zeiss Merlin or a VEGA TS 5130MM (TESCAN).

TEM/SAED

TEM was performed with a Philips CM30 ST (300 kV, LaB$_6$ cathode). The samples were suspended in *n*-butanol and drop-cast onto a lacey carbon film (Plano). The images were recorded with a CMOSS camera F216 (TVIPS)

XRPD

XRPD patterns were collected at room temperature on a Stoe Stadi-P Diffractometer (Cu-Kα1 (λ = 1.540596 Å), Ge(111) Johann monochromator, Mython 1K detector with an opening angle of 12.5°) in Debye-Scherrer geometry. The samples were measured inside sealed glass capillaries (φ 1.0 mm capillary from Hilgenberg, glass no. 14). For improved particle statistics the samples were spun. The samples were measured from 2° to 60° 2θ over 20 hours.

Structural refinement

The powder patterns were analyzed by Rietveld refinement[2] using the range from 2-30 ° 2θ with TOPAS V5. [3] The peak profile was described by applying the fundamental parameter[4] approach as implemented in TOPAS. The background was modeled with Chebychev polynomials and for the TBI-COF a 1/X background correction function was additionally used to describe the incoherent scattering at low 2θ. Lattice parameters were refined freely for TBI-COF and with constraints ($a=b$ and $\alpha = \beta$) for TTI-COF. For the TBI-COF a one layer structural model was refined, whereas for TTI-COF two layers were used and their shift with respect to each other was refined. The anisotropic peak shape, caused by stacking faults and mismatches in the microstructure, was modelled by a phenomenological model for microstrain.[5] In order to keep correlation to an absolute minimum the same constraints were used as for the lattice parameters using only used the S400 and S004 parameters.

Rwp is defined in TOPAS as:

$$R_{wp} = \left\{ \frac{\sum w_m (Y_{o,m} - Y_{c,m})^2}{\sum w_m Y_{o,m}^{\,2}} \right\}^{1/2} \quad (1)$$

with $Y_{o,m}$ and $Y_{c,m}$ being the observed and calculated data, respectively, at point m, w_m is the weighting which accounts for counting statistics by $w_m = 1/\sigma(Y_{o,m})^2$ with the error of intensity ($\sigma(Y_{o,m})$).

"The contour plot of the relative quality of refinement (Rwp) of the slipping direction in the TTI-COF was calculated by refining the XRPD using fixed α and β angles to obtain different layer offsets, but keeping the inter-layer distance constant. For the refinement, peak shapes were modeled with the use of particle size and strain-induced broadening. Such a simplified treatment of the refinement leads to different Rwp values than for the full refinement, hence the Rwp given in Fig. 3 can only be used in relative terms."

Disorder simulations

DIFFaX Simulations[6] were performed by construction of one layer unit cell based on the structural model of TBI-COF obtained by DFT calculations. The optimal stacking was taken from the offset present in the unit cell obtained from DFT. The simulation was performed for two opposing stacking directions, which was already enough to account for the observed change in the XRPD. The simulation included Gaussian broadening (0.15 trim). The stacking probability was varied sequentially from 99.9% uniform to 50%-50% random stacking, by the use of layer transition probabilities indifferent directions, as indicated next to the DIFFaX simulated XRPD pattern (Figure 4).

Theory

Quantum Espresso 5.1[7] was used for theoretical investigation of geometry-optimized unit cell and energy landscape. The Perdew-Burke-Ernzerhof (PBE) functional[8] was employed together with normconserving Martins-Troullier pseudopotentials.[9] The cut-off was set to 60 Ry and a 2 × 2 × 2 k-point grid was used for the unit cell

which included two COF sheets. A semi-empirical van-der-Waals interaction was added to account for dispersive interactions between sheets.[10]

The energy landscape of two sheets displaced from their equilibrium position was calculated by using two isolated layers from the converged structural optimization and displacing laterally one layer with respect to the other by given distances. The layer-layer distance perpendicular to the a-b plane (along c*) was held constant. Single-point energy calculations were performed at each lateral displacement using the Gamma point only. The two layers were separated from the next unit cell along the z-direction by >15 Å of vacuum.

IR

Infrared spectra were recorded in attenuated total reflection (ATR) geometry on a PerkinElmer UATR Two Spectrometer equipped with a diamond crystal and a Perkin Elmer Spectrum BX II FT-IR Spectrophotometer equipped with an ATR unit (Smith Detection Dura-Sample IIR diamond).

Sorption

Sorption measurements were performed on a Quantachrome Instruments Autosorb iQ MP with Argon at 87K.

Tables

Table S1: Obtained values for the Pawley refinement of the TTI-COF for different models. a) This value could not be refined due to the lack of reflections containing a c component. Therefore this value was fixed at the distance obtained from the force field geometry optimization.

	TTI-eclipsed	TTI-oblong	TTI-slipped	TBI-eclipsed
Schematic representation				
Restraints & constraints	$a=b\neq c$; $\alpha = \beta =90°$, $\gamma =120°$.	$a\neq b\neq c$; $\alpha = \beta = 90°$, $\gamma =120°$.	$a=b\neq c$; $\alpha = \beta$, $\gamma =120°$.	$a=b\neq c$; $\alpha = \beta =90°$, $\gamma =120°$.
Rwp	9.319	5.359	4.461	1.365
a (Å)	25.272 (19)	25.390 (6)	26.029 (6)	24.359 (3)
b (Å)	25.272 (19)	24.175 (6)	26.029 (6)	24.359 (3)
c (Å)	3.545 (8)	3.4997 (12)	3.5190 (8)	3.5[a]
α (°)	90	90	80.180 (12)	90
β (°)	90	90	80.180 (12)	90
γ (°)	120	120	120	120

Table S2: Unit cell parameters for the refined and calculated structures. The XRPD refinement was performed with a one layer unit cell. The DFT was done with a two layer unit cell to compare alternate and parallel direction stacking.

	TTI-COF			TBI-COF		
Unit cell parameter	XRPD Rietveld Refinement	DFT (imine parallel)	DFT (imine antiparallel)	XRPD Rietveld Refinement	DFT (imine parallel)	DFT (imine antiparallel)
a (Å)	25.840963	25.488	25.551	24.336(0.003)	25.702	25.780
b (Å)	25.884321	25.476	25.583	24.336(0.003)	25.612	25.500
c (Å)	7.101546	7.084	6.988	7.0	7.126	7.046
α (°)	83.64200	77.616	76.933	90	71.622	73.856
β (°)	82.93933	77.464	77.699	90	88.458	89.380
γ (°)	121.57261	119.882	120.380	120	119.978	119.621

Figures:
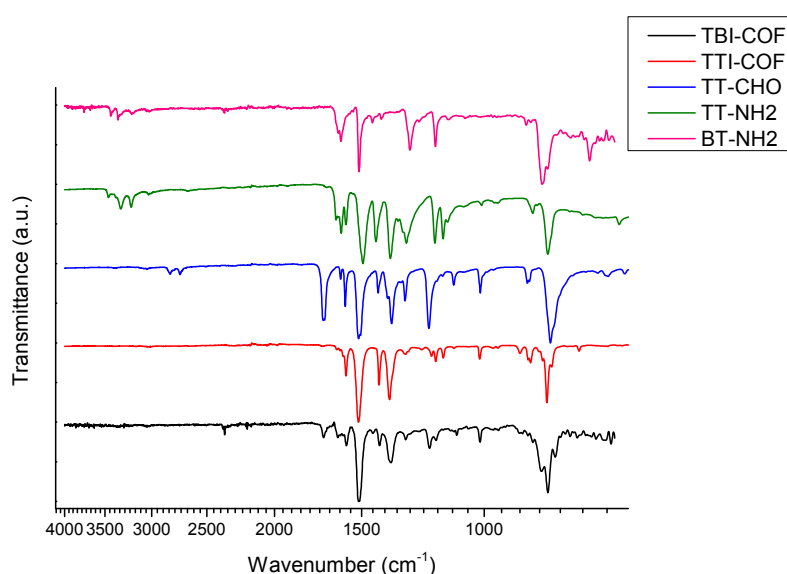
Figure S1: IR spectra of the TTI-COF and the TBI-COF show the transformation of the aldehyde and amine precursors to the corresponding imines. This is evident by the disappearance of the C=O stretch (1698 cm^{-1}) and the CO-H vibrations (2819 and 2730 cm^{-1}) in the precursor aldehyde (TT-CHO), the disappearance of the N-H vibrations (3500-3200 cm^{-1}) of the TT-NH2 precursor and (3500-3200 cm^{-1}) of the TB-NH2 precursor, as well as the appearance of the imine C=N stretch TTI-COF (1628 cm^{-1}) and TBI-COF at (1621 cm^{-1}).
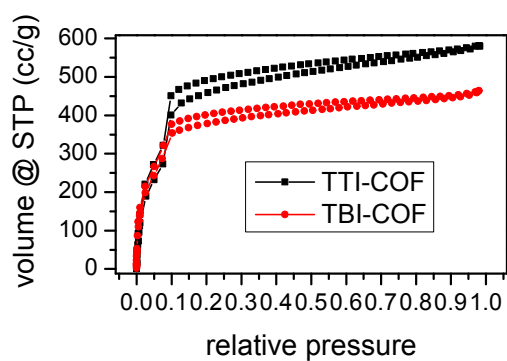
Figure S2: Sorption isotherms with Argon at 87K (right) of the TBI and the TTI-COF
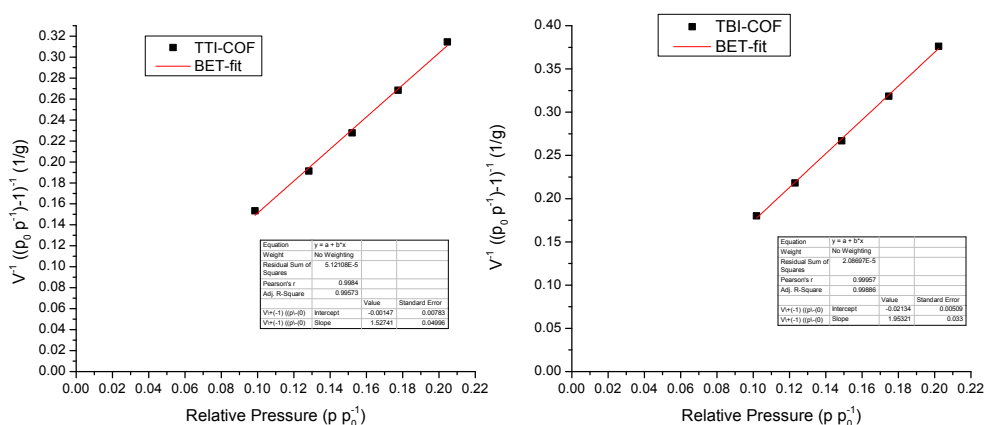
Figure S3: BET fit of the TTI-COF (left) and the TBI-COF (right).

"C3" pores

"oblong" pores
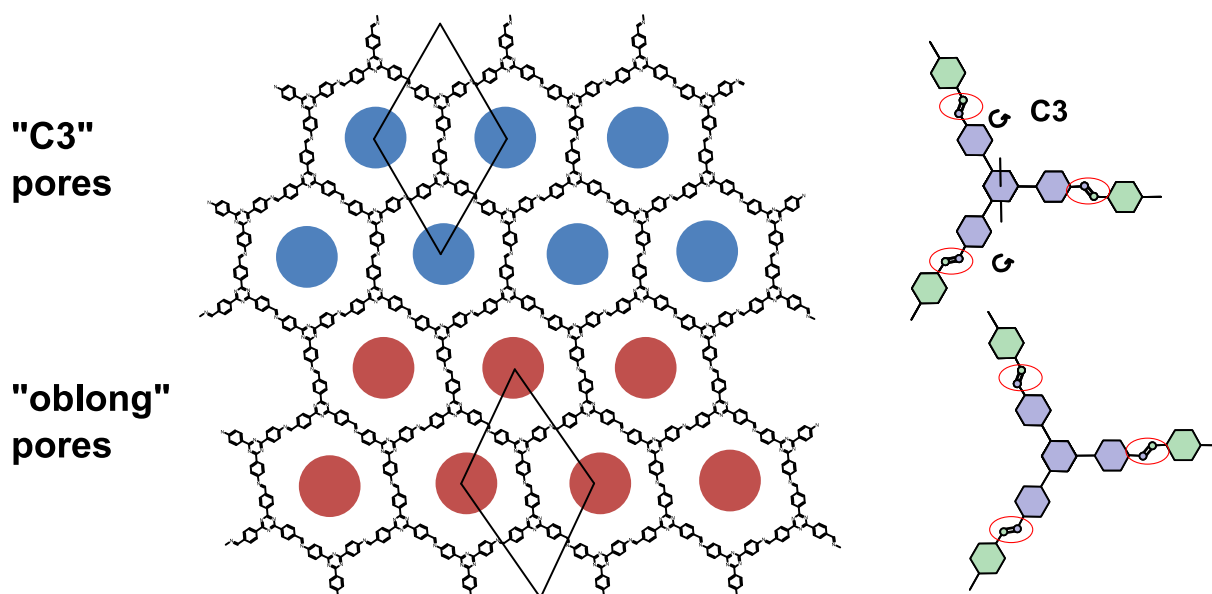
Figure S4: Illustration of the different possible relative orientations of the imine groups that could lead to different conformations. While the "C3" pores are only composed of imines with a rotational symmetry (right drawings), the imines in the "oblong" pores are rotated clockwise and anticlockwise.
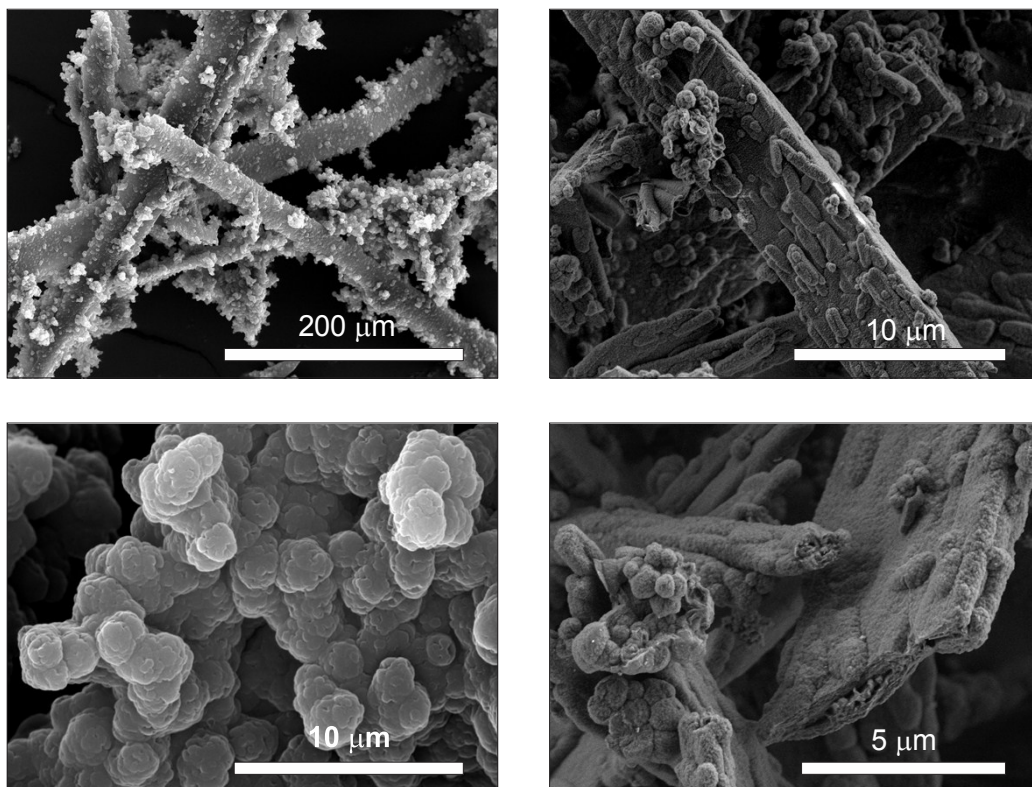
Figure S5: SEM images of the two COFs: TTI-COF on the left, TBI-COF on the right.
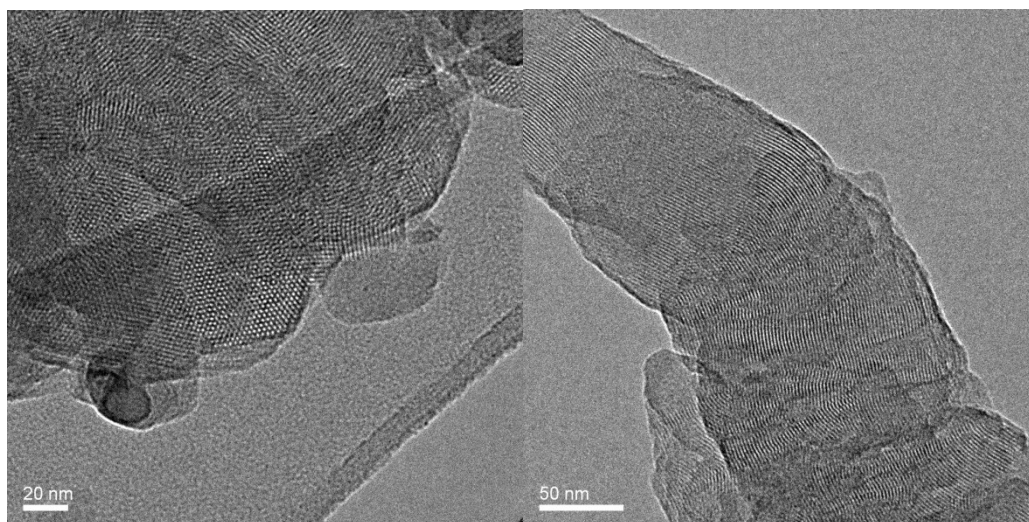
Figure S6: TEM images of the TTI-COF showing the hexagonal pore structure (left) and the bending of the crystallites/pores (right).
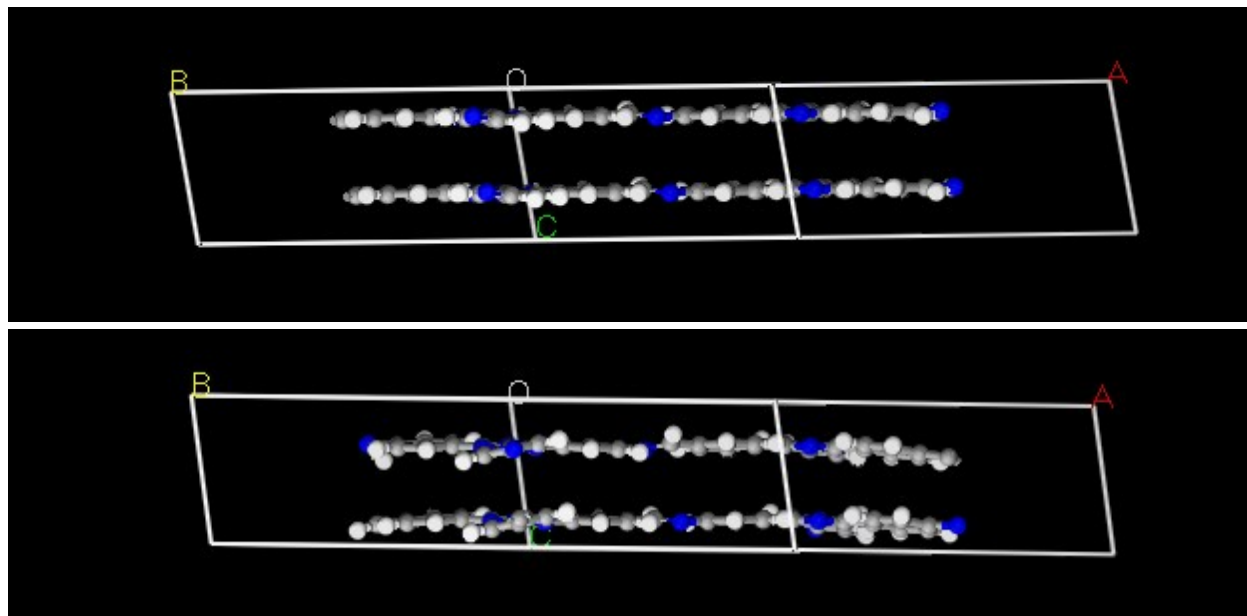
Figure S7: Visualization of the view of the TTI-COF perpendicular to the stacking direction with parallel imines (top) and antiparallel imines (bottom) as obtained from the periodic boundary DFT calculations.

Supporting References:

1. V. S. Vyas, M. Vishwakarma, I. Moudrakovski, F. Haase, G. Savasci, C. Ochsenfeld, J. P. Spatz and B. V. Lotsch, *Adv. Mater.*, 2016, DOI: 10.1002/adma.201603006, n/a-n/a.
2. H. Rietveld, *J. Appl. Crystallogr.*, 1969, **2**, 65-71.
3. *Journal*, 2014.
4. A. Coelho, *J. Appl. Crystallogr.*, 2000, **33**, 899-908.
5. P. Stephens, *J. Appl. Crystallogr.*, 1999, **32**, 281-289.
6. M. M. J. Treacy, J. M. Newsam and M. W. Deem, *Proceedings of the Royal Society of London. Series A: Mathematical and Physical Sciences*, 1991, **433**, 499-520.
7. P. Giannozzi, S. Baroni, N. Bonini, M. Calandra, R. Car, C. Cavazzoni, D. Ceresoli, G. L. Chiarotti, M. Cococcioni, I. Dabo, A. Dal Corso, S. de Gironcoli, S. Fabris, G. Fratesi, R. Gebauer, U. Gerstmann, C. Gougoussis, A. Kokalj, M. Lazzeri, L. Martin-Samos, N. Marzari, F. Mauri, R. Mazzarello, S. Paolini, A. Pasquarello, L. Paulatto, C. Sbraccia, S. Scandolo, G. Sclauzero, A. P. Seitsonen, A. Smogunov, P. Umari and R. M. Wentzcovitch, *Journal of physics. Condensed matter : an Institute of Physics journal*, 2009, **21**, 395502.
8. J. P. Perdew, K. Burke and M. Ernzerhof, *Phys. Rev. Lett.*, 1996, **77**, 3865-3868.
9. N. Troullier and J. L. Martins, *Physical review. B, Condensed matter*, 1991, **43**, 1993-2006.
10. S. Grimme, *J. Comput. Chem.*, 2006, **27**, 1787-1799.